Chem Soc Rev

Molecular Wires – Impact of π-Conjugation and Implementation of Molecular Bottlenecks

Journal:	*Chemical Society Reviews*
Manuscript ID:	CS-REV-07-2014-000262.R1
Article Type:	Review Article
Date Submitted by the Author:	30-Jul-2014
Complete List of Authors:	Schubert, Christina; Friedrich-Alexander-Universitaet Erlangen-Nuernberg, Department of Chemistry and Pharmacy Margraf, Johannes; Friedrich-Alexander-Universität Erlangen-Nürnberg Nägelsbachstraße 25, Friedrich-Alexander-Universität Erlangen-Nürnberg Clark, Tim; Friedrich-Alexander-Universität Erlangen-Nürnberg , Guldi, Dirk; Physical Chemistry, Department of Chemistry

Journal Name

RSCPublishing

ARTICLE

Molecular Wires – Impact of π-Conjugation and Implementation of Molecular Bottlenecks

Cite this: DOI: 10.1039/x0xx00000x

C. Schubert,[a] J. T. Margraf[b], T. Clark[b] and D. M. Guldi[a]

Received ooth January 2012,
Accepted ooth January 2012

DOI: 10.1039/x0xx00000x

www.rsc.org/

In this review we highlight recent progress in the field of photochemically and thermally induced electron transport through molecular bridges as integrative parts of electron donor-bridge-acceptor conjugates. The major emphasis is hereby on the design and the modular composition of the bridges. To this end, we will demonstrate that control over attenuation factors and reorganization energies, on one hand, as well as electronic and electron-vibration couplings, on the other hand, enables tuning electron transport over distances as short as 3.5 Å and as large as 50 Å by up to nine orders of magnitude. In terms of electron transport, the maximum extreme is given by carbon-bridged oligo-*p*-phenylenevinylenes of different lengths, while a zinc tetraphenylporphyrin free base tetraphenylporphyrin constitutes the minimum extreme.

Introduction

The search for suitable molecular structures and a fundamental understanding of their function in nanoscale devices play a key role in the rapidly emerging field of molecular electronics such as optoelectronics, solar energy conversion, molecular switches, and transistors.[1,2] A comprehensive understanding of electron-transfer and –transport processes, especially in molecular wires, is essential for future progress in many diverse fields of science.

At the molecular level, a wire is a structure through which electrons can be transported/transferred from one end to the other. Such a concept calls for probing electron transfer through single molecules. Two different types of experiments are typically employed for this purpose. On the one hand, conductance measurements including molecularly controllable break junctions and SAMs sandwiched between two electrodes provided a wealth of information. In this context, the reader is directed to a number of excellent reviews for further insight into the field of single-molecule conductance and SAM experiments.[3,4] On the other hand, in photoinduced electron-transfer reactions, one can imagine the electrodes of a break-junction experiment to be replaced by appropriate electron donors and acceptors. The electron transfer between these electron donors and acceptors is then mediated by a bridge unit. Therefore, electron donor-bridge-acceptor (D–B–A) conjugates (Figure 1) have served as model systems probing charge transfer processes on the molecular scale. In this review, we will only concentrate on photoinduced electron transfer experiments, as shown schematically in Figure 1.

Linear π-conjugated oligomers with well-defined chemical structures are best suited as linkers in conjugates such as that shown in Figure 1. In this review, the effect of varying parameters such as the nature of the bridging unit, the redox potentials of the end groups, intramolecular distances (*i.e.* length of the bridge), chemical functionalization of the different building blocks (*i.e.* linkage), and bottlenecks in between the bridging units are discussed.

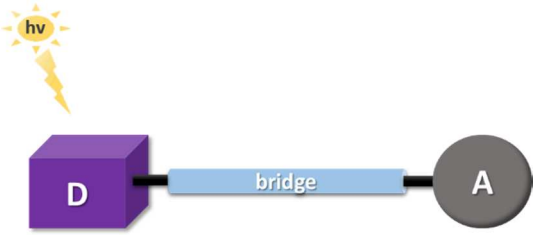

Figure 1 Covalently connected electron donor-bridge-acceptor (D-B-A) conjugate.

Therefore, we highlight and compare the electron-transfer properties of different D-B-A conjugates in terms of electronic coupling between the electron donors and acceptors via the corresponding bridges, attenuation factors, and reorganization energies. Mapping the local electron affinity onto an electron isodensity surface that corresponds approximately to the van der Waals surface provides decisive and mechanistic insights into the postulated electron-transfer features.

General Considerations about Electron Transfer Reactions

The Marcus theory provides the basis for relating the rate constant for electron transfer (k_{ET}) to thermodynamic parameters. In particular, these parameters are the underlying driving force $-\Delta G^0$ for electron transfer in different solvents, the

reorganization energy λ, and the electronic coupling V as it exists between electron donors and acceptors. Classical Marcus theory predicts a parabolic dependence of the plot of electron transfer rates (k_{ET}) versus $-\Delta G^0$ – Equation 1.

Such parabolae are typically divided into three regions: firstly, the region in which the rate constant increases with increasing thermodynamic driving force ($-\Delta G^0 < \lambda$), generally referred to as the normal region. Secondly, the top of the parabola ($-\Delta G^0 = \lambda$), where the reaction is activationless and the rate is at its maximum. It is basically controlled by the magnitude of electronic coupling V between the electron donors and acceptors. Thirdly, the region, where increasing the driving force even further results in an actual slow-down of the reaction rate ($-\Delta G\ ^0 > \lambda$). Such a highly exergonic range is generally referred to as the Marcus inverted region.[5]

$$k_{ET} = \sqrt{\left(\frac{4\pi^3}{h^2 \lambda k_B T}\right)}\ |V|^2 \exp\left[-\frac{\left(\Delta G^0 + \lambda\right)^2}{4\lambda k_B T}\right] \qquad \text{Eq. 1}$$

Optimal conditions for electron transfer demand charge-separation kinetics located at the top of the Marcus parabola and charge-recombination rates shifted far into the inverted region and, hence, their deceleration. Thus, small reorganization energies are desirable.

In contrast, the semi-classical Marcus theory divides λ into solvent (λ_S) and vibrational reorganization energies (λ_V) – Equation 2. Here, ω relates to the averaged frequency of the coupled quantum mechanical vibration modes and S is the electron-vibration coupling, leading to higher rate constants in the Marcus inverted region than expected from the classical Marcus theory.

$$k_{ET} = \sqrt{\left(\frac{4\pi^3}{h^2 \lambda_S k_B T}\right)}\ |V|^2 \sum_{v}^{\infty} \frac{e^{-S} S^v}{v!} \exp\left[-\frac{\left(\Delta G^0 + \lambda_S + v\hbar\omega\right)^2}{4\lambda_S k_B T}\right],$$

$$S = \frac{\lambda_v}{\hbar\omega} \qquad \text{Eq. 2}$$

In D-B-A systems the bridge plays a mediating role and provides coupling between the electron donors and acceptors. The fact that the magnitude of V depends on the nature of the bridge offers the possibility to control the electron transfer rate of through-bond electron transfer by structural means.

Excitation of the electron donors or acceptors, may result in a charge transfer from the photoexcited donor to the acceptor or from donor to the photoexcited acceptor through the bridge, respectively. The mechanism of this process is determined by the electron acceptor and donor energy levels of the involved moieties. These are typically approximated by the energy of the highest occupied and lowest unoccupied molecular orbitals (HOMO and LUMO).

Two contrasting cases, in which the energy levels of the LUMO of the bridge relative to the LUMO levels of the electron donor play a decisive role, should be considered. These are, on one hand, superexchange, in which the LUMO energy level of the bridge is significantly higher in energy than that of the donor and, on the other hand, electron hopping, in which the LUMO level of the bridge is energetically accessible from the donor energy levels – Figure 2.

Varying the bridge lengths allows distance dependent charge transfer rates to be measured with the aim of elucidating the hopping and superexchange charge-transfer regimes within molecular systems. Considering the latter, electron transfer from the electron donor to the acceptor proceeds via ‘‘virtual’’ acceptor states localized on the bridge, even though the bridge itself does not act as a real intermediate in the electron-transfer process – Figure 2. The rate of charge separation and/or recombination is then reflected by the electron-transfer rate constant k_{ET}, which decays exponentially with the distance between electron donor and acceptor:

$$k_{ET} = k_0 \times e^{-\beta R_{DA}} \qquad \text{Eq. 3}$$

Here, k_0 is the rate constant at the van der Waals contact distance of 3.5 Å, R_{DA} the distance between the electron donor and acceptor, and β is the so-called attenuation factor or damping factor. The latter quantifies the capability of a π-conjugated wire-like oligomer to transport electrical charges and, therefore, becomes a bridge-specific parameter. β should be as low as possible to promote rapid and efficient charge-transfer reactions.

A key factor hereby is the π-conjugation, which not only includes the conjugation within the molecular wire itself but also between the molecular wire and the electroactive termini. In other words, the coupling depends strongly on the relative energy levels and the energy gaps between electron donor and bridge and between bridge and electron acceptor.

For instance, Scott *et al*., have investigated oligomers such as *p*-phenylene bridges (Ph_n) (n = 1–5), fluorenone (n = 1–3) (FN_n), and *p*-phenylethynylene (n = 1–3) (PE_n) covalently attached to a 3,5-dimethyl-4-(9-anthracenyl) julolidine (DMJ-An) electron donor and a naphthalene-1,8:4,5-bis(dicarboximide) (NI) electron acceptor to rationalize how the charge-transport mechanism depends on the molecular structure.[6] Typical values for β range, on one hand, from 1.0 to 1.4 $Å^{-1}$ for protein structures and, on the other, from 0.01 to 0.04 $Å^{-1}$ for highly π-conjugated bridge structures. In vacuum, values of β are relatively large in the range of 2.0 to 5.0 $Å^{-1}$.[7]

Alternatively, a hopping mechanism occurs when the molecular bridge is energetically accessible for charge injection – Figure 2. In this case, charges reside on the bridge for a finite time and rates hardly depend on the distance (1/r). In general, the superexchange mechanism is preferred in short bridges and at low temperatures, while the hopping mechanism is seen for long bridges and at higher temperatures. The mechanism can be determined from the temperature dependence of the rate constants; strong temperature dependence suggests a thermally activated hopping mechanism, from which the activation barrier (E_a) is derived via the slope.

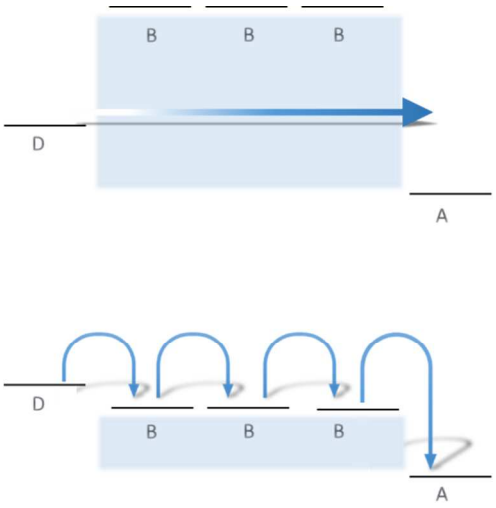

Figure 2 Schematic illustrations of tunneling (top) and hopping (bottom) mechanisms as modus operandi in charge-transfer reactions in D-B-A conjugates.

Short Range Charge Transfer in C_{60}–ZnP Model Conjugates – π-Stacked *trans*-2-ZnP-C_{60} and MP-C_{60} Conjugates

A useful model to study short-distance electron charge transfer in ZnP-C_{60} conjugates is the π–π stacked *trans*-2-**ZnP–C_{60}** system, in which a *trans*-2 addition pattern forces a close proximity between electron donor and electron acceptor.[8] In these cases, the double linkage enforces a face-to-face orientation between C_{60} and ZnP and, in turn, leads to a scenario, in which intramolecular charge-separation dominates over the competing energy transfer from the photoexcited ZnP to C_{60}. π-Stacking the electron donor above the acceptor has been demonstrated to keep the reorganization energy relatively low and to stabilize the charge-separated state in a variety of solvents.

The latter evolved as a probate means to change the free energy for charge separation and recombination over a wide range. For example, the lifetime of the charge-separated state decreases from 619 ps in toluene to 38 ps in benzonitrile. Considering that charge recombination yields the singlet ground state in both cases, the rates are clearly located in the Marcus-inverted region.

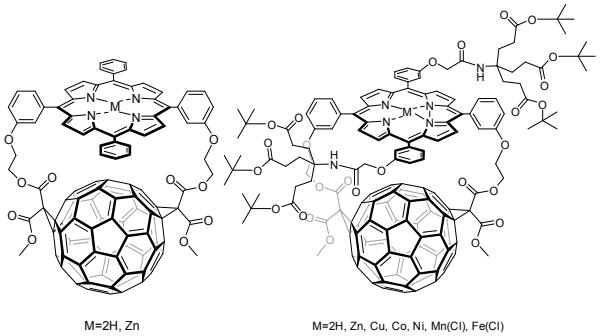

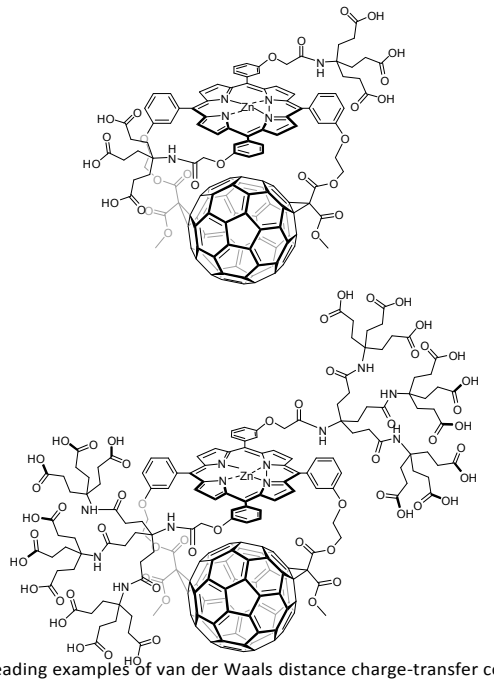

Figure 3 Leading examples of van der Waals distance charge-transfer conjugates: *trans*-2-**MP-C_{60}** with M = 2H, Zn and first generation dendronized *trans*-2-**MP-C_{60}** with M = 2H, Zn, Cu, Co, Ni, Mn(Cl), Fe(Cl) (top) and first and second generation dendronized *trans*-2-**ZnP-C_{60}**.

Correlating the rate constants with the thermodynamic driving forces for charge separation and recombination by plotting log k_{ET} versus $\Delta G_{ET}°$, leads to a parabolic dependence, from which an experimental λ value of 0.86 eV and an extremely strong electronic coupling (V) of 313 cm^{-1} were derived. An illustration is given in Figure 4.

Changing the metal center in the metalloporphyrin from zinc(II) to cobalt(II) – *trans*-2-**Co(II)P–C_{60}** – lowers the one-electron reduction potential of C_{60} by 40 mV, indicating significant electronic interactions between the π-system of C_{60} and the central cobalt(II). Two different oxidation products were found besides $C_{60}^{\bullet-}$ in the charge-separated state; either a metal-centered Co(III)P or a ligand-centered $Co(II)P^{\bullet+}$.[9] Interestingly, depending on the nature of the oxidation, that is, Co(III)P versus $Co(II)P^{\bullet+}$, the lifetime of the charge-separated state is increased by three orders of magnitude.

Moreover, a series of different metalloporphyrins bearing manganese(III), iron(III), nickel(II), and copper(II) have also been investigated – Figure 4.[10] In all these conjugates, a key feature is the short distance separating the excited-state electron donor from the acceptor. This *π-π* stacking motif has emerged as a powerful tool for overcoming the intrinsically fast deactivation of the excited states in metalloporphyrins that feature manganese(III), iron(III), nickel(II), and copper(II). The lifetimes of the rapidly and efficiently generated charge-separated state were found to depend on the solvent polarity and on the metal species.

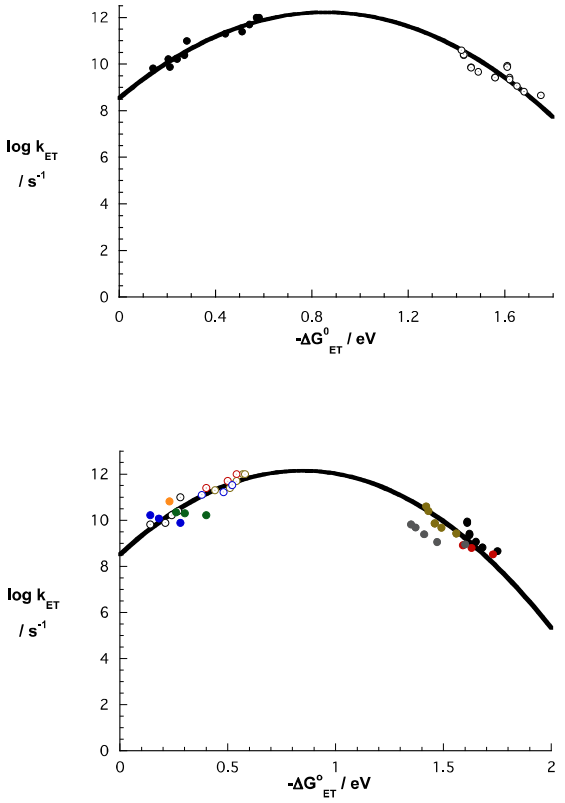

Figure 4 Above: driving force ($-\Delta G^0_{ET}$) dependence of the rate constants for charge separation and recombination for *trans*-2-**ZnP-C$_{60}$** in various solvents. Below: driving force ($-\Delta G^0_{ET}$) dependence of the rate constants for charge separation and recombination for *trans*-2-**MP-C$_{60}$** with **M**=**Mn(III)Cl** (blue symbols), **Fe(III)Cl** (orange symbols), **Co(II)** (grey symbols), **Ni(II)** (green symbols), **Cu(II)** (red symbols), **Zn(II)** (brown symbols), **H$_2$** (black symbols) in various solvents.

Again, the dependence of rate constants on the driving force of electron transfer yields information about the reorganization energy (0.84 eV) and the electronic coupling (70 cm^{-1}). Both closely resemble the values seen for the π–π stacked *trans*-2-**ZnP–C$_{60}$** system. Local electron affinity calculations[11] illustrate the strong electronic interaction in this system. Figure 5 represents the local electron affinity (EA_L) map of *trans*-2-**ZnP–C$_{60}$** with projected onto a 0.03 a.u electron isodensity surface.

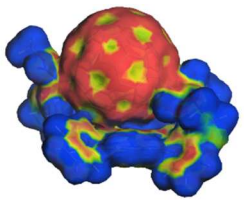

Figure 5 EA_L mapped from -80.0 (blue) to -30.0 kcal mol^{-1} (red) onto the electronic density isosurface (0.03 e$^-$ bohr^{-3}) of *trans*-2-**ZnP-C$_{60}$**.

The need for water-soluble fullerenes in biomedical technologies has directed research towards the development of suitable synthetic routes to overcome the hydrophobicity of C_{60}. Ruppert *et al.*[12] showed that deprotection of the terminal dendritic ester groups in dendronized porphyrins attached to C_{60} through a *trans*-2 addition pattern results in a new class of truly water-soluble conjugates. These tightly coupled *trans*-2-**ZnP–C$_{60}$** electron donor-acceptor conjugates allow the control of charge separation and charge recombination dynamics by modifying the size of the dendrimer (*i.e.,* first *versus* second generation).

Unlike the assays in organic solvents – *vide supra* – the decay depends strongly on the dendrimer generation and is multi-exponential. These results imply the role of different dendrimer rotamers. Different, competitively formed $ZnP^{\bullet+}$-$C_{60}^{\bullet-}$ species with varying stability are formed. Addressing this, quantum chemical calculations suggest shielding effects of the electroactive moieties that vary in the different conformers. The position of the dendrimer relative to ZnP depends strongly on the generation. The preferred conformation of the first generation dendrimer places both dendrimers above the ZnP plane and, in turn, shields the latter. In contrast, in the second generation dendrimer, the size and the number of negative charges of the dendritic arms ensure interactions with ZnP and C_{60} and no preference of shielding was seen. The charge-separated state is therefore stabilized in the first generation dendrimer due to the shielding of the most susceptible ZnP. Moreover, a larger donor–acceptor distance was found for the first generation dendrimers, which also favors longer-lived charge-separated states.

Long Range Charge Transfer in C_{60}–ZnP Conjugates

Early work by Guldi *et al.* describes successful long-range electron-transfer realized by combining several redox-active building blocks – linking ferrocene (Fc) and zinc tetraphenylporphyrin (ZnP) to free base tetraphenylporphyrin (H_2P) and C_{60} – to form **ZnP–C$_{60}$**, **ZnP–H$_2$P–C$_{60}$**, and **Fc–ZnP–H$_2$P–C$_{60}$** conjugates – Figure 6.

In the latter, ZnP performs as an antenna that transfers its singlet excited-state energy to the energetically lower lying H_2P. This energy transfer is followed by a sequential electron-transfer relay evolving from the generated singlet excited state of H_2P to yield the adjacent $H_2P^{\bullet+}/C_{60}^{\bullet-}$. Then the intermediate $ZnP^{\bullet+}/C_{60}^{\bullet-}$ and, finally, the distant $Fc^{\bullet+}/C_{60}^{\bullet-}$ charge-separated states are generated. Local electron-affinity calculations confirm the electron-transfer pathway from ZnP to H_2P and finally to C_{60}. Figure 7 shows the local electron affinity map of **ZnP–H$_2$P–C$_{60}$**.

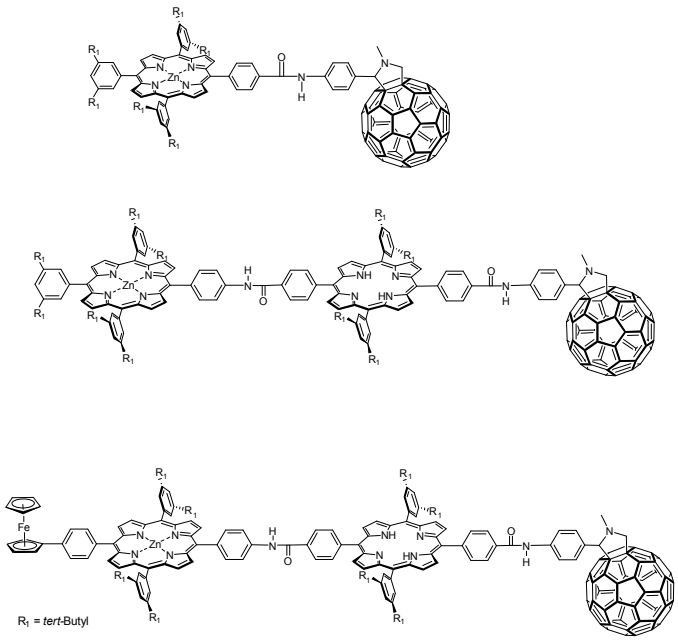

Figure 6 Leading examples of long distance charge transfer conjugates: **ZnP-C_{60}**, **ZnP-H_2P-C_{60}**, and **Fc-ZnP-H_2P-C_{60}**.

Fc–ZnP–H_2P–C_{60}, thus, mimics all the primary events seen in photosynthesis upon photoexcitation, that is, light harvesting, energy transfer, electron transfer, and charge shift. Further advances in terms of efficiency and lifetime involve substitution of H_2P by ZnP.

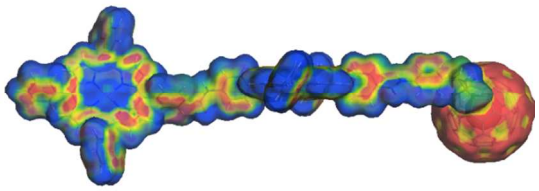

Figure 7 EA_L mapped from -80.0 (blue) to -30.0 kcal mol^{-1} (red) onto the electronic density isosurface (0.03 e^- $bohr^{-3}$) of **ZnP–H_2P–C_{60}**.

On one hand, this raises the excited-state energy of the electron donor from approximately 1.89 to 2.04 eV. On the other hand, the oxidation potential of the electron donor is lowered by nearly 300 mV. These factors result in larger -ΔG° values for the initial electron transfer and, in turn, higher efficiencies and outstanding charge-recombination rate constants of 34% and 0.62 s^{-1} in **Fc–ZnP–ZnP–C_{60}**, respectively, when compared to **Fc–ZnP–H_2P–C_{60}**. In any of these cases, the reorganization energies depend strongly on the electron donor-acceptor distance. This increases from **ZnP–C_{60}** and **ZnP–H_2P–C_{60}** to **Fc–ZnP–H_2P–C_{60}** with values ranging from 0.66 to 1.32 eV.

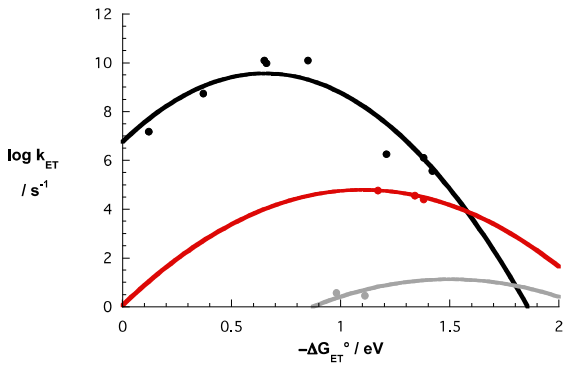

Figure 8 Driving force (-ΔG°) dependence of intramolecular ET rate constants in **ZnP-C_{60}** (black), **Fc-ZnP-C_{60}**, **Fc-H_2P-C_{60}**, **ZnP-H_2P- C_{60}** (red), and **Fc-ZnP-H_2P-C_{60}** (grey). The lines represent the best fit (**ZnP-C_{60}**, λ = 0.66 eV, **Fc-ZnP-C_{60}**, **Fc-H_2P-C_{60}**, and **ZnP-H_2P-C_{60}**, λ = 1.09 eV, **Fc-ZnP-H_2P-C_{60}**, λ = 1.32 eV).

Figure 8 summarizes the Marcus plots of these conjugates, where the final electron donors (Fc) and the primary electron acceptors (C_{60}) are separated by distances of up to 50 Å. Calculating the attenuation factor (β) from the distance dependence of the rate constants of **Fc–ZnP–H_2P–C_{60}** (~50 Å), **ZnP–H_2P–C_{60}** (~30 Å), and **ZnP–C_{60}** (~12 Å) yields a rather high β value of 0.60 $Å^{-1}$. In addition, the electronic coupling, V, is as small as 5.6×10^{-5} cm^{-1}.[13]

This example reveals by far the longest lifetime ever reported for intramolecular charge recombination in synthetic electron donor-acceptor conjugates featuring porphyrins and fullerenes. This value is also comparable to the lifetime (~1 s) of the bacteriochlorophyll dimer radical cation ($(Bchl)_2^{\bullet+}$)-secondary quinone radical anion ($QB^{\bullet-}$) ion pair in bacterial photosynthetic reaction centers.[14]

Usually, long-distance electron transfer is considered to be a nonadiabatic process. Its rate is determined by a combination of strongly distance-dependent tunneling and weakly distance dependent incoherent transport events. Tunneling obeys a superexchange mechanism, in which the bridge acceptor states are considered solely as a coupling medium that never accommodates any charges, in contrast to the situation described above for **Fc–ZnP–H_2P–C_{60}**. Incoherent electron transfer involves real intermediate states that couple to internal nuclear motions of the bridge and the surrounding medium.

To design molecular bridges capable of facilitating long-range electron-transfer reactions, a number of aspects should be considered. Firstly, the conjugation influences the π-system and the electronic coupling between electron donor and acceptor governs the electron transfer rates. Secondly, the molecular wire-like behavior is driven by the attenuation factors. Thirdly, the impact of the total reorganization energies stem from both the electron donors and the electron acceptors.

In the light of the latter, special interest lies on electron donor–acceptor conjugates that incorporate ZnP as electron donor and C_{60} as acceptor, linked by π-conjugated oligomers of variable length. The combination of ZnP and C_{60} ensures small

reorganization energies because of the highly delocalized ZnP radical cations and C_{60} radical anions.[15] Moreover, focusing on the same electron donor-acceptor moieties provides a way to compare the impact of different molecular bridges.

It is well documented that the attenuation factor is a function of electronic structure and overall architecture of the bridge. Thus, much effort has been devoted to designing bridges that facilitate long-range electron transfer reactions. In this context, π-conjugated oligomers are interesting candidates, which led to the investigations of ZnP and C_{60} connected by alkynes, *p*-phenyleneethylenes (o*p*PE), fluorenes (oFl), *p*-phenylenevinelynes (o*p*PV), etc. – *vide infra*.

Long Range Charge Transfer in C_{60}–Wire–ZnP Conjugates

Vail *et al.*[16] showed that one to three alkyne units bridging ZnP and C_{60} leads to an extension of the π-conjugation over the entire length of the bridge. Mainly long-range charge separation (7.8×10^9 s^{-1}) and recombination (1.9×10^6 s^{-1}) events took place as shown in transient absorption experiments. A superexchange mechanism is proposed as the operative mode for electron transfer, owing to LUMO(ZnP)–LUMO(wire) gaps greater than 0.3 eV and LUMO(C_{60})–LUMO(wire) gaps of at least 1.0 eV.

Slower rates for charge recombination in tetrahydrofuran *versus* benzonitrile clearly indicated that charge-recombination events are occurring in the Marcus inverted region. Analysis of the distance dependence revealed attenuation factors of 0.06 $Å^{-1}$. Notably, these attenuation factors are in excellent agreement with values found in earlier studies.[17] The changes in the reduction potentials of the D-B-A conjugates compared with suitable models show that ZnP as electron donor and C_{60} as electron acceptor are indeed electronically coupled – at least to some extent. These findings proved that even triple bonds are effective mediators regarding long-range electronic interactions up to nearly – but not limited to – 24 Å.

Including phenyl groups between the triple bonds impacts the extended π-conjugation and, in turn, the charge-transfer properties, as shown by Lembo *et al.*[18] In β-substituted **ZnP–*p*-phenyleneethynylene–C_{60}** – Figure 7 – charge separation occurs in polar media to afford a long-lived charge-separated state with rate constants for charge separation of 1.68×10^8 s^{-1} and charge recombination of 0.84×10^6 s^{-1}. Transient absorption and cyclic voltammetry studies did not reveal accessible oxidized states of the bridge. Therefore, electron transfer via a superexchange mechanism seems to be the most probable operative mode.

Absorption measurements, on one hand, and cyclic voltammetry studies, on the other, suggest that complete extension of the porphyrin HOMO along the whole length of the linker should be excluded. Thus, the conformation of the porphyrin relative to the phenyl rings of the bridge is decisive in terms of preventing full conjugation between the electron donor and the linker. Still, oligo-ethynylenephenylenes feature a rather effective wire-like behavior resulting from a possible coplanarity between the phenyl rings – Figure 9.

Another aspect is the matching of the HOMO/LUMO energy levels of the different constituents in the D-B-A conjugates. They play a major role for efficient electronic communication between electron donor and acceptor, as also shown by quantum chemical and electrochemical investigations. Linear dependence of the electron-transfer rate constant on the electron donor-acceptor distance likewise yields a low attenuation factor of 0.11 $Å^{-1}$. This value complements those reported in previous studies, taking the attenuation factor β of 0.21 $Å^{-1}$ into account, which was found in similar systems bearing π-extended tetrathiafulvalene (*ex*TTF) as electron donors.[19] Notably, the wire-like behavior depends on the substitution pattern and on the donor features. Very similar damping factors, namely 0.29 $Å^{-1}$, have recently been reported by Albinsson *et al.*[20]

Oligofluorenes of different lengths have also been reported as molecular wires connecting ZnP to C_{60} – Figure 9.[21] Calculations have shown that systems with large electron donor-acceptor distances feature charge separation via incoherent charge hopping. The decreasing LUMO energies of the bridge are mainly responsible for this trend. In contrast, decreasing the oFL length seems to activate a superexchange tunneling due to closer electron donor-acceptor spacing.

Temperature-dependent photophysical experiments demonstrated that the charge-transfer mechanism is also controllable by temperature. Both charge separation and recombination processes are compatible with a molecular wire behavior for oFLs and with an attenuation factor β of 0.097 $Å^{-1}$. This wire-like behavior is well in line with the local electron-affinity maps, as illustrated in Figure 9. The addition of a phenyl ring between ZnP and wire perturbs the homogeneous oFL π-conjugation and, in turn, creates a bottleneck for electrons to pass. For that reason, charge separation is slower, while charge recombination is faster. Both trends are reflected in increased β values.

In stark contrast, the incorporation of vinylene spacers into **exTTF–oligofluorene–C_{60}** conjugates has been shown both experimentally and theoretically to improve the charge-transfer features to yield a β value of 0.075 $Å^{-1}$. Enhanced π-conjugation caused by higher orbital overlap is responsible for this trend. Similar results stem from studies, in which Fcs have been linked in four different ways to oFLs.[22] Here, the Fc moiety is linked to oFL – firstly, directly without any spacer, secondly, by an ethynyl linkage, thirdly, by a vinylene linkage, and, fourthly, by a p-phenylene unit.

The mode of linkage has a profound effect. For example, intramolecular charge separation is found to occur rather independently of the distance. Hereby, the linker between Fc and oFL acts as a bottleneck and significantly impacts the intramolecular charge-separation rates, resulting in β_{CS} values between 0.08 and 0.19 $Å^{-1}$. Charge recombination, on the other hand, depends strongly on the electron-donor–acceptor distances, but not at all on the linkers. A value for β_{CR} of 0.35 $Å^{-1}$ was found in the analysis of all of the aforementioned systems. In general, different linkers and different fullerene

functionalization exert marked impacts on the electronic interactions between the electroactive units.[23,24]

Among all the functional oligomers, *oligo*(phenylenevinylene)s (o*p*PVs) have gained the most attention with respect to efficient charge transport reactions because they exhibit attenuation factors as low as 0.01 $Å^{-1}$.[25] Vital for the wire like behavior is that the HOMO energies of C_{60} match those of the long *p*-phenylenevinylene bridges. This facilitates charge injection into the wire. Equally important is the strong electronic coupling, realized through the *para*-conjugation in *p*-phenylenevinylenes.

Local electron-affinity calculations confirm these findings. Especially with respect to oFLs and o*p*PVs, local electron-affinity maps as they are shown in Figure 7, show that the electron affinity is fairly homogeneously distributed throughout the whole bridge, whereas in o*p*PEs local maxima (red) and minima (yellow), seen on the phenyl rings and triple bonds, respectively, alternate.

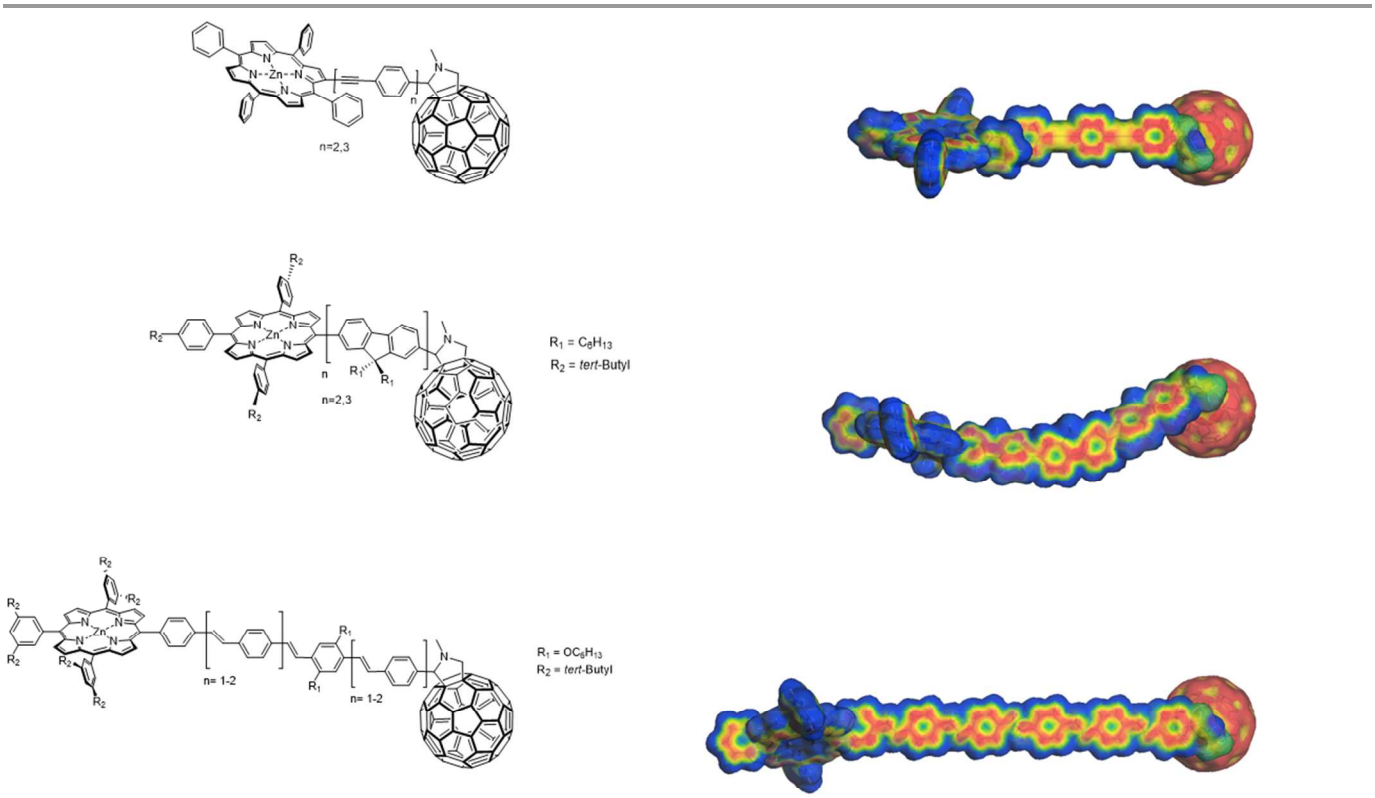

Figure 9 Left: leading examples of molecular wire conjugates: **ZnP–*p*-phenyleneethynylene–C_{60}**, **ZnP–fluorene–C_{60}**, and **ZnP-*p*-phenylenevinylene-C_{60}**. Right: EA_L mapped from -80.0 (blue) to -30.0 kcal mol^{-1} (red) onto the electronic density isosurfaces (0.03 e^- $bohr^{-3}$) - displaying the differences between the three different molecular-systems.

In **ZnP–*p*-phenylenevinylene–C_{60}** – Figure 9 – the charge separation process evolving from photoexcited ZnP was confirmed by means of transient absorption spectroscopy and the k_{CS} values were calculated to be 3.2 - 4.5 × 10^9 s^{-1} for D-B-A conjugates of different lengths. As for the charge recombination, the k_{CR} values were reported to be in the range from 0.9 × 10^6 to 4.5 × 10^6 s^{-1} in benzonitrile and THF at room temperature. Considering edge-to-edge distances as large as 39.0 Å, such rate constants are only feasible if good electronic coupling between ZnP and C_{60} is guaranteed. As a matter of fact, electron donor-acceptor electronic couplings of ~2.0 cm^{-1} assist electron transfer reactions, which give rise to shallow distance dependences and small attenuation factors of 0.03 $Å^{-1}$.

It is remarkable that these features are realized despite the rotational freedom of the donor–bridge and bridge–acceptor linkages. The Marcus fits of the charge-separation and -recombination kinetics give a total reorganization energy of 0.72 eV with o*p*PV trimers and pentamers, which correspond to electron donor-acceptor distances of 25 and 39 Å, respectively.[26]

To analyze the charge-recombination mechanism, experiments between 268 and 365 K were conducted. A weak temperature dependence in the 268 to 300 K range suggests that a stepwise charge recombination can be ruled out, leaving electron tunneling via superexchange as the modus operandi. This

picture is in sound agreement with the thermodynamic barrier to formation of **ZnP–*p*-phenylenevinylene$^{\bullet+}$–C$_{60}^{\bullet-}$**.

At temperatures higher than 300 K, the situation changes and charge recombination is accelerated. The observed strong temperature dependence suggests a thermally activated charge recombination. In particular, the activation barriers (E_a), derived from slopes, are 0.2 eV.[27]

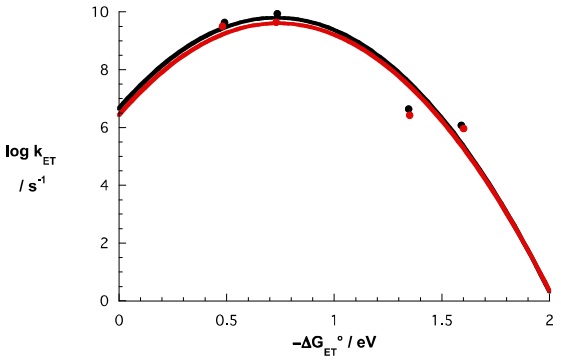

Figure 10 Driving force (-ΔG^0_{ET}) dependences of the rate constants for charge separation and charge recombination for **ZnP-o*p*PV$_3$-C$_{60}$** (black) and **ZnP-o*p*PV$_5$-C$_{60}$** (red).

Compared to oligovinylene bridges, these small energy differences suggest that the observed small β_{CS} and β_{CR} values must be attributed to the high electron transferring ability of oligophenylenevinylenes. Please note that β_{CS} values larger than 0.08 Å^{-1}were reported by Osuka *et al.,*[28] for oligovinylene bridges. A possible conclusion is that the phenyl groups among the vinylene units do not retard electron transfer. Instead, phenyl groups, as they are placed between vinylene units, seem to promote remote electron migration.

As k_{CS} values for **exTTF–oligophenylenevinylene–C$_{60}$** are in the same range as those for **ZnP–o*p*PV–C$_{60}$**, the main factor determining the β_{CS} value, which is with 0.01 Å^{-1} slightly lower in **exTTF–oligophenylenevinylene–C$_{60}$**, may be the higher electron delocalization along the HOMO of the oligophenylenevinylene than that of the LUMO.[29] Relative to our previous observation on exTTF-trimer-C$_{60}$, with an experimentally determined activation barrier of 0.5 eV, the smaller energy gap in **ZnP–o*p*PV–C$_{60}$** reflects the lower HOMO of ZnP relative to exTTF.

Fine Tuning o*p*PVs

Ever since o*p*PVs have emerged as a benchmark for efficient charge transport due to their extraordinary low attenuation factors, modifications of their structure have documented its enormous impact on the electronic properties.

To this end, we demonstrated recently that the insertion of [2,2´]paracyclophane into o*p*PV bridges leads to a molecular junction-like behavior, resulting in a facilitated charge transfer in one direction, that is, from C$_{60}$ to ZnP via *p*Cp, but a disfavored charge transfer in the other direction, that is, from ZnP to C$_{60}$ via *p*Cp. This originates from the fact that *p*Cps break the through-bond conjugation, leading to different β values for charge separation (β_{CS}) of 0.039 Å^{-1} and recombination (β_{CS}) of 0.045 Å^{-1}.[30]

As a complement to the latter, charge-transport properties through *p*Cp-o*p*PV wires comprising one, two, and three *p*Cps, were probed – Figure 11.[31] ZnP excitation results in a rather slow charge transfer between ZnP and C$_{60}$. In contrast, C$_{60}$ excitation leads exclusively to a charge transfer between the first *p*Cp and C$_{60}$ without giving rise to a subsequent charge shift to yield the **ZnP$^{\bullet+}$–*p*Cp–o*p*PV–C$_{60}^{\bullet-}$** charge-separated state.

Temperature dependent ZnP singlet excited state decays, that is, fluorescence and transient absorption experiments, corroborate that in the low temperature range – below 303 K – the rate constants do not change, suggesting that a superexchange mechanism is the modus operandi, while in the high temperature range – above 303 K – the rate constants increase.

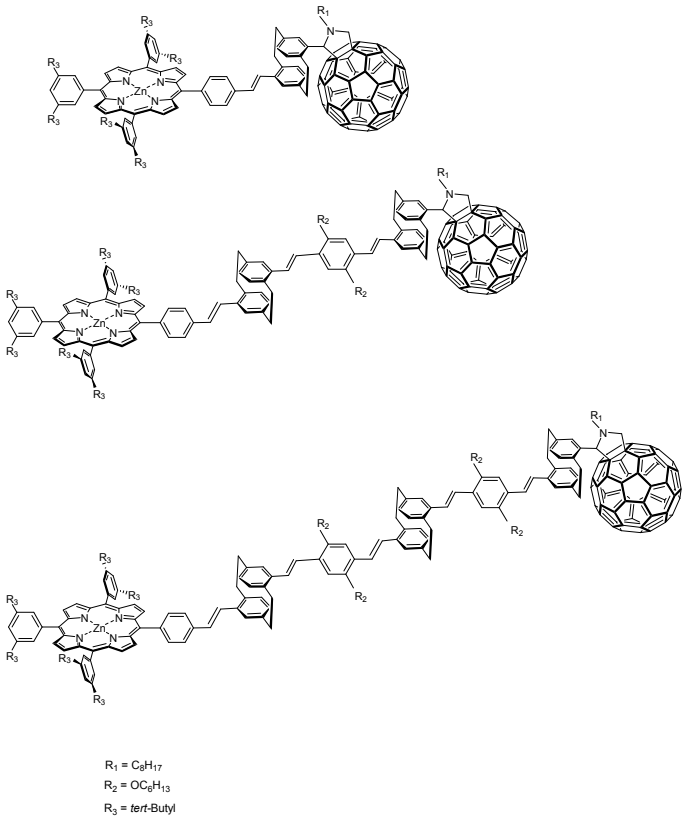

Figure 11 Leading examples of molecular wire conjugates: **ZnP–(*p*Cp-o*p*PV)–C$_{60}$**, **ZnP–(*p*Cp-o*p*PV)$_2$–C$_{60}$**, and **ZnP–(*p*Cp-o*p*PV)$_3$–C$_{60}$**.

Moreover, relating the charge-separation dynamics to the electron donor-acceptor separation enabled us to evaluate the attenuation factor of the *p*Cp-o*p*PV bridges. Rather strong distance dependence for **ZnP–*p*Cp–o*p*PV–C$_{60}$** and **ZnP–(*p*Cp–o*p*PV)$_2$–C$_{60}$** featuring an attenuation factor of 0.145 Å^{-1} is followed by weak distance dependence for **ZnP–(*p*Cp–o*p*PV)$_2$–C$_{60}$** and **ZnP–(*p*Cp–o*p*PV)$_3$–C$_{60}$** with a value of 0.012

$Å^{-1}$. Here, local electron-affinity maps show a distribution throughout the entire molecule with through-space conjugation across the *p*Cps.

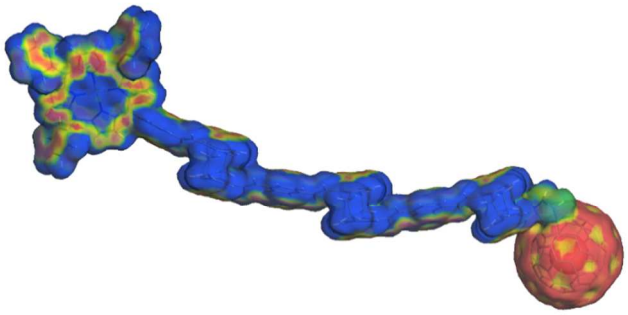

Figure 12 EA_L mapped from -80.0 (blue) to -30.0 kcal mol^{-1} (red) onto the electronic density isosurface (0.03 e^- $bohr^{-3}$) of **ZnP–(*p*Cp-o*p*PV)$_3$–C$_{60}$**.

Another strategy to control electron transfer rates is by modulating the reorganization energy. This was shown for the first time in non-covalent ensembles rather than covalent conjugates by coordination of ZnP to pyridyl groups in short and long o*p*PVs bearing C_{60}, namely **C$_{60}$–pyr**, **C$_{60}$–o*p*PV1–pyr** and **C$_{60}$–o*p*PV3–pyr**, respectively (Figure 13).

Photoexcitation of ZnP leads to the formation of charge-separated states, that is, the one-electron oxidized ZnP radical cation and the one-electron reduced C_{60} radical anion. In both instances, the charge-separated states are metastable with, however, **C$_{60}$–o*p*PV3–pyr•ZnP** showing a faster charge recombination than **C$_{60}$–o*p*PV1–pyr•ZnP**, despite the larger electron donor-acceptor separation.

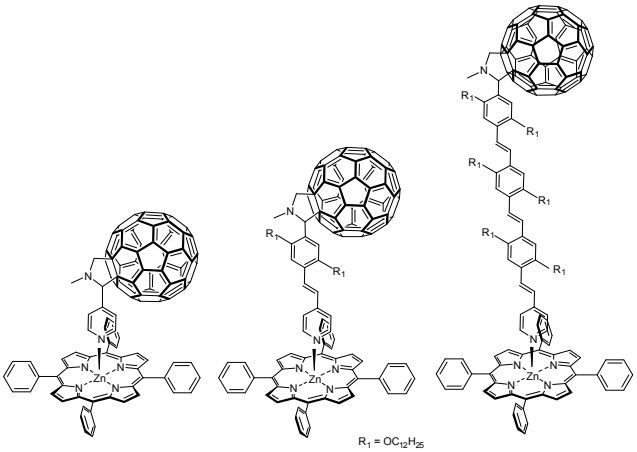

Figure 13 Leading examples of molecular wire ensembles: **C$_{60}$-pyr·ZnP**, **C$_{60}$-o*p*PV1-pyr·ZnP**, and **C$_{60}$-o*p*PV3-pyr·ZnP**.

This rather surprising result stems from a distinct distance dependence found for **C$_{60}$–o*p*PV1-pyr•ZnP** and **C$_{60}$–o*p*PV3-pyr•ZnP** with electron donor-acceptor distances of 16.8 and 30 Å and with reorganization energies of 0.74 and 0.91 eV, respectively – see Figure 14.

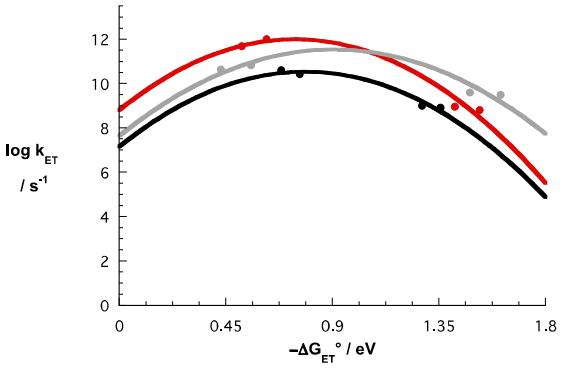

Figure 14 Driving force ($-\Delta G^0_{ET}$) dependences of the rate constants for charge separation and charge recombination for **C$_{60}$-o*p*PV1-pyr·ZnP** (red), **C$_{60}$-o*p*PV3-pyr·ZnP** (grey), and **C$_{60}$-pyr·ZnP** (black).

In contrast, as seen before[27], linking ZnP covalently to **C$_{60}$–o*p*PVs** at, for example, electron donor-acceptor distances between 24.9 and 38.7 Å leads to invariant reorganization energies of around 0.72 eV – Figure 8. This difference goes hand in hand with changes in the attenuation factor with values as low as 0.03 $Å^{-1}$ for the covalently linked conjugates and as high as 0.24 $Å^{-1}$ for **C$_{60}$–o*p*PV1-pyr•ZnP** and **C$_{60}$–o*p*PV3-pyr•ZnP**. Insights into these differences came from molecular modeling, which disclosed that the fairly homogeneous pathway for electrons from the electron donating ZnP to the electron accepting C_{60} is suddenly disrupted at the pyridinic nitrogen – Figure 15.

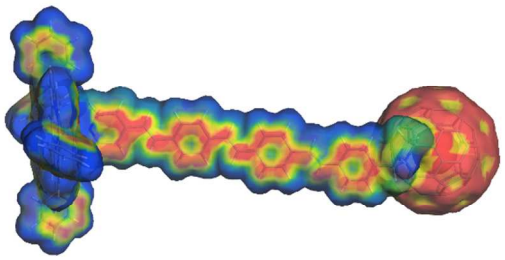

Figure 15 EA_L mapped from -80.0 (blue) to -30.0 kcal mol-1 (red) onto the electronic density isosurface (0.03 e- $bohr^{-3}$) of **C$_{60}$-o*p*PV3-pyr·ZnP**.

The lowest-lying singlet charge-transfer state of **C$_{60}$–pyr·ZnP** shows significant deviations from the ground state geometry that move the charged moieties closer together. These distortions result in the charged fullerene moiety moving approximately 1 Å closer to one of the twisted phenyl substituents, allowing stabilization by CH…C hydrogen bonding, which is quite favorable in this case because of the negative charge on the fullerene.

Implementing such bottlenecks enables the reorganization energy in non-covalent ensembles to be modulated and, therefore, opens new perspectives for the design and

preparation of new architectures potentially efficient for energy applications.[26]

A general disadvantage of *p*-phenylene (o*p*P), *p*-phenyleneethylenes (o*p*PE), and *p*-phenylenevinylenes (o*p*PV) is the ability to rotate around the single bonds that connect the individual phenyl units. This causes a deviation from planarity along the oligomer chain.[27] Moreover, in all these examples electronic coupling, that is, the effectiveness of the π-conjugation, controls the molecular wire behavior.

In contrast, electron-vibration coupling is usually neglected, primarily because electron transfer excites only low-energy torsional motions of C–C σ-bonds rather than vibrations of the C–C π-skeleton. Therefore, elastic tunneling/superexchange and hopping mechanisms, which occur much more slowly than inelastic tunneling, dominate charge transfer through conventional molecular wires. Interestingly, Marcus theory predicts potentially fast electron-transfer reactions – even in the Marcus inverted region – which arise from electron-vibration (e-v) coupling throughout the bridge. Hitherto, the lack of suitable organic wires has hampered experimental verification.

To rule out the effect of deviation from planarity along the oligomer chain, rigid and flat carbon-bridged oligo-*p*-phenylenevinylene (Co*p*PV) wires were synthesized. In a recent study[32] we investigated D-B-A conjugates with ZnP as electron donor, C_{60} as electron acceptor, and carbon-bridged oligo-*p*-phenylenevinylene (Co*p*PV) of different lengths as bridges (Figure 16).

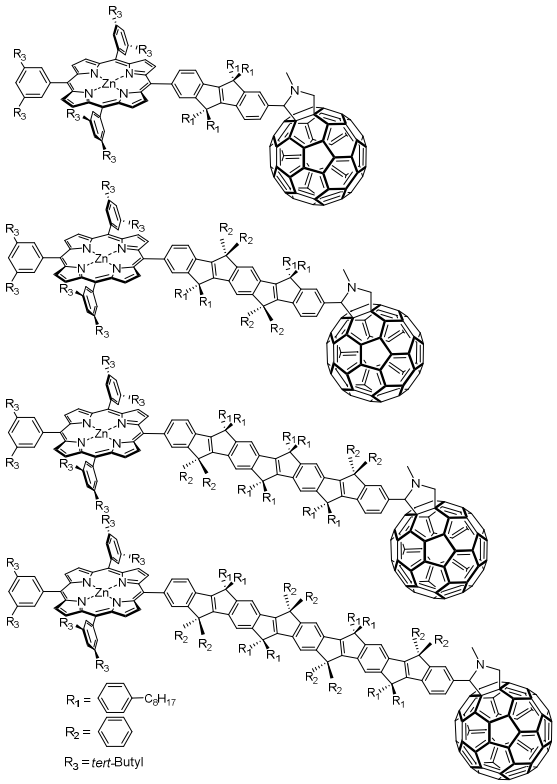

Figure 16 Leading examples of molecular wire conjugates: **ZnP–Co*p*PV$_1$–C$_{60}$**, **ZnP–Co*p*PV$_2$–C$_{60}$**, **ZnP–Co*p*PV$_3$–C$_{60}$**, and **ZnP–Co*p*PV$_4$–C$_{60}$**.

Charge separation evolves for **ZnP–Co*p*PV*n*–C$_{60}$** (n = 1 and 2) in THF and anisole. In contrast to the latter, the formation of **ZnP–Co*p*PV*n*$^{\bullet+}$–C$_{60}^{\bullet-}$** (n = 3 and 4) governs the excited-state dynamics in THF and anisole. Importantly, in more polar solvents such as benzonitrile, the formation of **ZnP$^{\bullet+}$–Co*p*PV*n*–C$_{60}^{\bullet-}$** (n = 1–4) was found to dominate the overall photoreactivity. **ZnP–Co*p*PV3–C$_{60}$** exhibited an 840-fold increase in electron transfer rate compared with **ZnP–o*p*PV3–C$_{60}$**[27] in the Marcus inverted region, where e–v coupling greatly affects the electron transfer. These new Co*p*PVs feature rigidity as well as planarity, both of which are crucial criteria favoring strong e-v coupling and, in turn, enabling inelastic electron tunneling.

The plot of electron transfer rates (k_{ET}) versus driving forces for electron transfer ($-\Delta G^0_{ET}$) in different solvents sheds light on the strength of the electronic couplings (V = 24 ± 7 cm^{-1} for **ZnP–Co*p*PV2–C$_{60}$**) and the total reorganization energies (λ = 0.89 ± 0.04 for **ZnP–Co*p*PV2–C$_{60}$**). V is enhanced as expected due to the flatness of the wire. The reorganization energy is larger for this more rigid molecule compared to **ZnP–o*p*PV3–C$_{60}$** – see Figure 17.

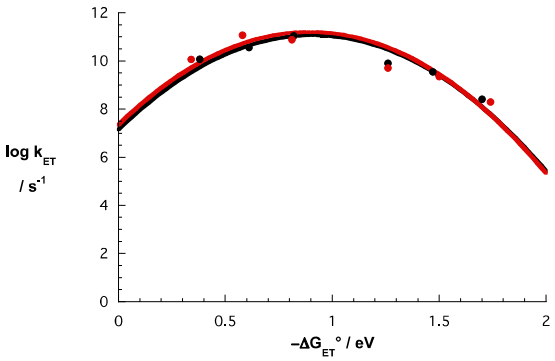

Figure 17 Driving force ($-\Delta G^0_{ET}$) dependences of the rate constants for charge separation and charge recombination for **ZnP–Co*p*PV1–C$_{60}$** (black) and **ZnP–Co*p*PV2–C$_{60}$** (red).

The attenuation factors for CS (β_{CS}) and CR (β_{CR}) in Co*p*PVs are similar to those seen for o*p*PVs. In benzonitrile, β_{CS} is 0.056 ± 0.002 and β_{CR} is 0.078 ± 0.006 Å^{-1}.

Furthermore, local electron-affinity calculations confirm the electron-transfer pathway from the electron donor via the bridge to the electron accepting C_{60}. Figure 18 shows the local electron-affinity map of **ZnP–Co*p*PV4–C$_{60}$** with constant high electron-affinity path throughout the molecule.

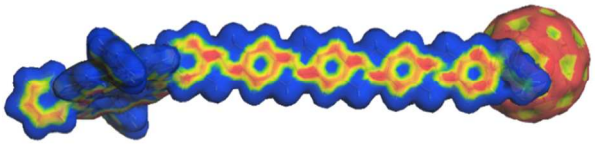

Figure 18 EAL mapped from -80.0 (blue) to -30.0 kcal mol-1 (red) onto the electronic density isosurfaces (0.03 e- bohr^{-3}) of **ZnP–Co*p*PV4–C_{60}**.

This study on a rational design of π-conjugation provides clear experimental evidence that the rigidity of the π-system strengthens e-v coupling. Importantly, the strained array of two fused five-membered rings locked into the π-skeleton together with six-membered rings is undoubtedly responsible for the rigidity of the system. Inelastic electron tunneling has so far only been observed for molecular wires fixed onto substrates and at extremely low temperatures.[33] Thus, the emergence of such an electron-transfer pathway in solution at room temperature is remarkable, suggesting that Co*p*PVs may be utilized for molecular devices that operate under practically useful conditions.

Conclusions

In this review, photoinduced electron transfer and the mechanism of charge transport in molecular wires together with their determining factors is highlighted. The impact on the electronic properties by chemically tuning molecular wires is outlined. Particular attention has been paid to the electronic coupling between electron donor and acceptor, the molecular wire-like behavior in terms of attenuation factor, and the total reorganization energies because these factors govern the electron-transfer rates. We mainly focused on electron-donor-acceptor conjugates, which incorporate ZnP as electron donors and C_{60} as electron acceptors, linked by π-conjugated oligomers of precise length and constitution. Special emphasis is placed on oligophenylenevinylene and how small changes in the structure of these π-conjugated oligomers lead to profound differences in the π-conjugation and hence, different electronic properties of the molecular-wire conjugates. Molecule-assisted transport is a fundamental process and systematic exploration of these systems should help to realize molecular wires for new optoelectronic devices – including molecular electronics, printable electronics, etc.

Acknowledgements

J.T. Margraf is supported by a Beilstein Foundation Scholarship. The Deutsche Forschungsgemeinschaft (Cluster of Excellence Engineering of Advanced Materials) is acknowledged.

Notes and references

[a] Department of Chemistry and Pharmacy & Interdisciplinary Center for Molecular Materials (ICMM), Friedrich-Alexander-Universität Erlangen-Nürnberg, Egerlandstrasse 3, 91058 Erlangen, Germany.
[b] Computer-Chemie-Centrum, Department of Chemistry and Pharmacy & Interdisciplinary Center for Molecular Materials (ICMM), Friedrich-Alexander-Universität Erlangen-Nürnberg, Nägelsbachstr. 25, 91052 Erlangen, Germany

† Footnotes should appear here. These might include comments relevant to but not central to the matter under discussion, limited experimental and spectral data, and crystallographic data.

Electronic Supplementary Information (ESI) available: [details of any supplementary information available should be included here]. See DOI: 10.1039/b000000x/

1 M. G. Harrison, and R. H. Friend, *Electronic Materials: The Oligomer Approach*, Wiley-VCH, Weinheim, (1998) 515.
2 U. Mitschke, and P. Bäuerle, *J. Mater. Chem*., 2000, **10**, 1471.
3 (a) A. Aviram, and M. A. Ratner, *Chem. Phys. Lett*., 1974, **29**, 277. (b) R. H. M. Smit, Y. Noat, C. Untiedt, N. D. Lang, M. C. van Hemert and J. M. van Ruitenbeek, *Nature*, 2002, **419**, 906. (c) B. Q. Xu, and N. J. Tao, *Science*, 2003, **301**, 1221. (d) E. Lörtscher, *Nature Nanotechnology,* 2013, **8**, 381. (e) S. V. Aradhya and L. Venkataraman, *Nature Nanotechnology,* 2013, **8**, 399. (f) J. R. Heath, *Annu. Rev. Mater. Res*., 2009, **39**, 1. (g) K. Moth-Poulsen, and T. Bjørnholm, *Nat. Nanotechnol*., 2009, **4**, 551. (h) R. L. McCreery, and A. J. Berggren, *Adv. Mater*., 2009, **21**, 4303.
4 H. B Akkerman and B. de Boer, *J. Phys.: Condens. Matter*, 2008, **20**, 013001.
5 R. A.Marcus and N. Sutin, *Biochim. Biophys. Acta*, 1985, **811**, 265.
6 A. M. Scott, A. B. Ricks, M. T. Colvin and M. R. Wasielewski, *Angew. Chem.* 2010, **122**, 2966; *Angew. Chem. Int. Ed*. 2010, **49**, 2904.
7 E. A. Weiss, M. R. Wasielewski and M. A. Ratner, *Top. Curr. Chem*., 2005, **257**, 103.
8 D. M. Guldi, C. Luo, T. Da Ros, M. Prato, E. Dietel and A. Hirsch, *Chem. Commun.*, 2000, 375.
9 L. R. Sutton, M. Scheloske, K. S. Pirner, A. Hirsch, D. M. Guldi, and J.-P. Gisselbrecht, *J. Am. Chem. Soc.,* 2004, **126**, 10370.
10 F. Spänig, M. Ruppert, J. Dannhäuser, A. Hirsch, and D. M. Guldi, *J. Am. Chem. Soc.,* 2009, **131**, 9378.
11 B. Ehresmann, B. Martin, A. H. C. Horn, T. Clark, *J. Mol. Model.* 2003, **9**, 342.
12 M. Ruppert, F. Spänig, M. Wielopolski, C. M. Jäger, W. Bauer, T. Clark, A. Hirsch, and D. M. Guldi, *Chem. Eur. J.*, 2010, **16**, 10797.
13 (a) H. Imahori, D. M. Guldi, K. Tamaki, Y. Yoshida, C. Luo, Y. Sakata and S. Fukuzumi, *J. Am. Chem. Soc.,* 2001, **123**, 6617. (b) D. M. Guldi, H. Imahori, K. Tamaki, Y. Kashiwagi, H. Yamada, Y. Sakata and S. Fukuzumi, *J. Phys. Chem. A,* 2004, **108**, 541.
14 (a) J. Deisenhofer and J. R. Norris, *The Photosynthetic Reaction Center*; Academic Press: San Diego, (1993). (b) R.E. Blankenship, M.T. Madigan, C.E. Bauer (Eds.), *Anoxygenic Photosynthetic Bacteria*, Kluwer Academic Publishers, Dordrecht, The Netherlands (1995).
15 D. M. Guldi, B. M. Illescas, C. M Atienza, M. Wielopolski and N. Martín, *Chem. Soc. Rev*., 2009, **38**, 1587.
16 S. A. Vail, P. J. Krawczuk, D. M. Guldi, A. Palkar, L. Echegoyen, J. P. C. Tome, M. A. Fazio and D. I. Schuster, *Chem. Eur. J*., 2005, **11**, 3375.

17 (a) A. Osuka, N. Tanabe, S. Kawabata, I. Yamazaki, and N. Nishimura, *J. Org. Chem*. 1995, **60**, 7177. (b) V. Grosshenny, A. Harriman, and R. Ziessel, *Angew. Chem. Int. Ed.* 1995, **34**, *23/24, 2705.*
18 A. Lembo, P. Tagliatesta, D. M. Guldi, M. Wielopolski and M. Nuccetelli, *J. Phys. Chem. A*, 2009, **113**, 1779.
19 C. Atienza, N. Martin, M. Wielopolski, N. Haworth, T. Clark and D. M. Guldi, *Chem. Commun*., 2006, 3202.
20 (a) K. Pettersson, J. Wiberg, T. Ljungdahl, J. Martensson and B. Albinsson, *J. Phys. Chem. A*, 2006, **110**, 319. (b) K. Pettersson, A. Kyrychenko, E. Ronnow, T. Ljungdahl, J. Martensson and B. Albinsson, *J. Phys. Chem. A*, 2006, **110**, 310.
21 M. Wielopolski, G. Rojas, C. van der Pol, L. Brinkhaus, G. Katsukis, M. R. Bryce, T. Clark and D. M. Guldi, *ACS Nano*, 2010, **4**, 6449.
22 C. Schubert, M. Wielopolski, L.-H. Mewes, G. M. Rojas, C. van der Pol, K. C. Moss, M. R. Bryce, J. E. Moser, T Clark and D. M. Guldi, *Chem. Eur. J.,* 2013, **19**, 7575.
23 H. Li, C. Schubert, P. O. Dral, R. D. Costa, A. La Rosa, J. Thüring, S.-X. Liu, C. Yi, S. Filippone, N. Martín, S. Decurtins, T. Clark and D. M. Guldi, *ChemPhysChem*, 2013, **14**, 2910.
24 Y. Takano, C. Schubert, N. Mizorogi, L. Feng, A. Iwano, M. Katayama, M. A. Herranz, D. M. Guldi, N. Martín, S. Nagase and T. Akasaka, *Chem. Sci.,* 2013, **4**, 3166.
25 (a) W. B. Davis, W. A. Svec, M. A. Ratner, and M. R. Wasielewski, *Nature*, 1998, **396**, 60. (b) G. Pourtis, D. Beljonne, J. Cornil, M. A. Ratner, and J. L. Brédas, *J. Am. Chem. Soc.*, 2002, **124**, 4436. (c) K. Müllen, and G. Wegner (Eds.) *Electronic Materials: The Oligomer Approach,* Wiley-VCH, Weinheim, (1998). (d) R. E. Martin, and F. Diederich, *Angew. Chem.,* 1999, **111**, 1440; *Angew. Chem. Int. Ed*., 1999, **38**, 1350. (e) J.-F. Nierengarten, *Sol. Energy Mater. Sol. Cells*, 2004, **83**, 187. (f) J. L. Segura, N. Martín, and D. M. Guldi, *Chem. Soc. Rev.,* 2005, **34**, 31. (g) A. Hradsky, B. Bildstein, N. Schuler, H. Schottenberger, P. Jaitner, K.-H. Ongania, K. Wurst, and J.-P. Launay, *Organometallics,* 1997, **16**, 392. (h) N. Ono, H. Tomita, and K. Maruyama, *J. Chem. Soc. Perkin Trans. 1,* 1992, 2453.
26 C. Stangel, C. Schubert, S. Kuhri, G. Rotas, J. T. Margraf, E. Regulska, T. Clark, T. Torres, N. Tagmatarchis, D. M. Guldi, and A. G. Coutsolelos, *Chem. Sci*. submitted.
27 G. de la Torre, F. Giacalone, J. L. Segura, N. Martín and D. M. Guldi, *Chem. Eur. J.,* 2005 , **11** , 1267.
28 A. Osuka, N. Tanabe, S. Kawabata, I. Yamazaki and Y. Nishimura, *J. Org. Chem*., 1995, **60**, 7177–7185.
29 F. Giacalone, J. L. Segura, N. Martín and D. M. Guldi, *J. Am. Chem. Soc.*, 2004, **126**, 5340–5341.
30 A. Molina-Ontoria, M. Wielopolski, J. Gebhardt, A. Gouloumis, T. Clark, D. M. Guldi and N. Martín, *J. Am. Chem. Soc.,* 2011, **133**, 2370.
31 M. Wielopolski, A. Molina-Ontoria, C. Schubert, J. T. Margraf, E. Krokos, J. Kirschner, A. Gouloumis, T. Clark, D. M. Guldi and N. Martín, *J. Am. Chem. Soc.,* 2013, **135**, 10372–10381.
32 J. Sukegawa, C. Schubert, X. Zhu, H. Tsuji, D. M. Guldi and E. Nakamura, *Nature Chemistry*, 2014, accepted; doi:10.1038/nchem.2026
33 (a) S. Kubatkin, A. Danilov, M. Hjort, J. Cornil, J. L. Bredas, N. Stuhr-Hansen, P. Hedegard and T. Bjornholm, *Nature,* 2003, **425**, 6959, 698. (b) J. G. Kushmerick, J. Lazorcik, C. H. Patterson, R. Shashidhar, D. S. Seferos, and G. C. Bazan, *Nano Lett.,* 2004, **4**, 639. (c) E. A. Osorio, K. O'Neill, N. Stuhr-Hansen, O. F. Nielsen, T. Bjørnholm, and H. S. J. van der Zant, *Adv. Mater*., 2007, **19**, 281.

